Preprints of the 21st IFAC World Congress (Virtual)
Berlin, Germany, July 12-17, 2020

Multicopter Attitude Control through NMPC Design with Guaranteed Stability

Ngoc Thinh Nguyen * **Ionela Prodan** ** **Laurent Lefèvre** **

* *Univ. of Luebeck, Institute for Robotics and Cognitive Systems, Luebeck, Germany. Email:* nguyen@rob.uni-luebeck.de.
** *Univ. Grenoble Alpes, Grenoble INP* †*, LCIS, Valence, France. Email:* {ionela.prodan,laurent.lefevre}@ lcis.grenoble-inp.fr.
† *Institute of Engineering and Management Univ. Grenoble Alpes.*

Abstract: This paper presents an original NMPC (Nonlinear Model Predictive Control) design with guaranteed stability for the attitude set-point angle tracking of multicopters. The design is an extension of our previous work on stabilizing the NMPC scheme for "computed-torque like" systems by using terminal invariant set constructed under the CTC (Computed-Torque Control) controller. The novelty resides in the complexity reduction for the design process which is done by reducing the dependence of the required elements (e.g., the terminal region's radius, the Lipschitz constant) on the desired angle set-points which change fast and are not known in advance. The contributions are validated in simulation over a quadcopter model.

Keywords: Attitude control, set-point tracking, NMPC (Nonlinear Model Predictive Control), CTC (Computed-Torque Control), multicopter.

1. INTRODUCTION

Multicopters (also referred as *multirotors*) are already impacting our society: from assessing damage, locating victims in case of natural disasters to delivering pizzas, and more (Mogili and Deepak, 2018). Among various research directions related to the multicopters, the attitude control problem has raised much interest in both the research and the aerospace industrial communities (Nascimento and Saska, 2019) since stabilizing the attitude plays an essential role in controlling the vehicles. While conceptually simple, there are interesting intricacies due to the strongly nonlinear rotation dynamics, the singularities occurring at some specific configurations (e.g., upright position) as well as constraints on states and inputs. Various attitude control applications in the literature only assume that the controlled system will operate in the admissible range without any necessary enforcement (Freddi et al., 2011; Nguyen et al., 2017), which probably leads to constraints violation, invalid control inputs and even instability.

In view of these shortcomings, we propose in this paper an NMPC (Nonlinear Model Predictive Control) controller for tackling the attitude control problem under state and input constraints. The MPC approach is well-known for its capability of easily handling various constraints with a standard design while still providing good control performance (Mayne et al., 2000). Thanks to the advances in fast-solving methods (Badgwell and Qin, 2015), powerful solvers (Wächter and Biegler, 2006) and processors/microprocessors technologies, it has already become possible to employ MPC method for aerospace applications (Gros et al., 2012; Zanelli et al., 2018). However, there are still remaining issues on MPC design, such as stability and feasibility. For tackling these issues, two additional ingredients in the MPC scheme are reported in the literature: a terminal cost and a terminal constraint set (besides the standard indispensable stage cost). This design is facilitated by the existing designing rules presented in Mayne et al. (2000) which revolve around an important ingredient, usually hidden from the MPC scheme: a local controller, under which, the terminal constraint set is both admissible and positive invariant. In our previous work, Nguyen et al. (2019), we have exploited the CTC (Computed-Torque Control) law as the local controller to design the NMPC scheme for "computed-torque like" systems which stand for a broad range of systems, such as, aerospace crafts, robot arms and also the rotation dynamics of the multicopters. The method provides a larger invariant set and a better insight into the system's behavior (w.r.t. the standard approach using a linear controller (Chen and Allgöwer, 1998)).

In this paper, we apply the contributions in Nguyen et al. (2019) to design an NMPC controller for angle set-point tracking with guaranteed stability. The novelties lie in the several alternative designs for elements such as the Lipschitz constant and the efficient way to establish the terminal region. We reduce the dependence of the design on the desired set-points received from the high control level which are not known in advance, and hence, mitigate the complexity of the on-line solving process.

The paper is organized as follows. Section 2 presents the rotation dynamics of a standard multicopter system and the corresponding computed-torque controller. Next, Section 3 introduces the general NMPC scheme and summarizes the design principals for guaranteeing the closed-loop stability while the elements of the scheme are detailed in Section 4. Then, the simulation results are given and discussed in Section 5. Finally, Section 6 gives the conclusions and future works.

2. PRELIMINARIES

2.1 Rotation dynamics of a multicopter system

The rotation dynamics of a multicopter system is usually employed as those of a fully-actuated 3-dimensional rigid body (Freddi et al., 2011; Nguyen et al., 2017):

$$\dot{\eta} = W^{-1}\omega, \tag{1}$$

$$\dot{\omega} = J^{-1}\left(-\omega \times (J\omega) + u\right), \tag{2}$$

with $\eta \triangleq [\phi\ \theta\ \psi]^\top \in \mathbb{R}^3$, the roll, pitch, yaw angles and $\omega \triangleq [\omega_x\ \omega_y\ \omega_z]^\top \in \mathbb{R}^3$, the angle rates. The three input torques are gathered in $u \triangleq [u_\phi\ u_\theta\ u_\psi]^\top \in \mathbb{R}^3$ (i.e. the multicopter controls the three torques by changing the relative rotating speeds of its rotors). The inertia tensor is $J \triangleq \text{diag}\{J_x, J_y, J_z\} \in \mathbb{R}^{3\times 3}$ while the matrix $W \in \mathbb{R}^{3\times 3}$ and its inversion are explicitly given by:

$$W = \begin{bmatrix} 1 & 0 & -\mathrm{s}\,\theta \\ 0 & \mathrm{c}\,\phi & \mathrm{s}\,\phi\,\mathrm{c}\,\theta \\ 0 & -\mathrm{s}\,\phi & \mathrm{c}\,\phi\,\mathrm{c}\,\theta \end{bmatrix},\ W^{-1} = \begin{bmatrix} 1 & \mathrm{s}\,\phi\,\mathrm{t}\,\theta & \mathrm{c}\,\phi\,\mathrm{t}\,\theta \\ 0 & \mathrm{c}\,\phi & -\mathrm{s}\,\phi \\ 0 & \mathrm{s}\,\phi/\,\mathrm{c}\,\theta & \mathrm{c}\,\phi/\,\mathrm{c}\,\theta \end{bmatrix}, \tag{3}$$

with $\mathrm{s}(\cdot)$, $\mathrm{c}(\cdot)$, $\mathrm{t}(\cdot)$ denoting the trigonometric functions $\sin(\cdot)$, $\cos(\cdot)$, $\tan(\cdot)$, respectively. Furthermore, the system (1)–(2) is subject to its state and input constraints given as follows:

$$\mathcal{X} = \Big\{(|\phi|, |\theta|) \leq \phi_{\max},\ (|\omega_x|, |\omega_y|) \leq \omega_{\max}\Big\}, \tag{4}$$

$$\mathcal{U} = \Big\{|u| \leq u_{\max}\Big\}, \tag{5}$$

with $\phi_{\max} \in (0, \pi/2)$ the maximum angle value, $\omega_{\max} \in \mathbb{R}_+$ the maximum angle rate and $u_{\max} \in \mathbb{R}^3_+$ gathering the maximum values of three torques on three axes.

Remark 1. The condition $(|\phi|, |\theta|) \leq \phi_{\max} < \pi/2$ is sufficient to avoid singularities of the matrix W^{-1} as in (3) which happens at the perpendicular position, i.e., $\phi = \pi/2$ and $\theta = \pi/2$. Also, the roll, pitch angles (ϕ, θ) and the two angle rates (ω_x, ω_y) as in (4) can be constrained by different limits for each variable. However, it is customary to design the constraints as in (4) due to the symmetry of the multicopter system (Hehn and D'Andrea, 2015). In any case, different bounds for these parameters can be easily employed within our contributions. □

2.2 Computed-torque control law for attitude control

Computed-torque control (CTC) is a special application of feedback linearization control particularized for a broad range of robotics systems referred as "computed-torque like" systems which admit the Largrangian dynamics (Lewis et al., 2003; Craig, 2005). The CTC approach is widely applied for the attitude control problems (Freddi et al., 2011; Nguyen et al., 2017) which requires first to transform the system (1)–(2) into its "computed-torque like" formulation:

$$JW\ddot{\eta} + J\dot{W}\dot{\eta} + (W\dot{\eta}) \times (JW\dot{\eta}) = u, \tag{6}$$

which is obtained by introducing $\omega = W\dot{\eta}$ from (1) to the dynamics (2). Then, the CTC controller is given by:

$$u_{\text{CTC}} = JW\mu + J\dot{W}\dot{\eta} + (W\dot{\eta}) \times (JW\dot{\eta}), \tag{7}$$

in which, η and $\dot{\eta}$ are obtained as feedback from the system. The virtual input $\mu \in \mathbb{R}^3$ is usually designed using the well-known PD control method:

$$\mu = \ddot{\eta}_d + K_\eta e_\eta + K_{\dot{\eta}} e_{\dot{\eta}}, \tag{8}$$

with $e_\eta = \eta - \eta_d$, $e_{\dot{\eta}} = \dot{e}_\eta = \dot{\eta} - \dot{\eta}_d$ the errors on the angles and the angle derivatives. The gain matrices are chosen as $K_\eta = \text{diag}\{K_\phi, K_\theta, K_\psi\}$ and $K_{\dot{\eta}} = \text{diag}\{K_{\dot{\phi}}, K_{\dot{\theta}}, K_{\dot{\psi}}\}$ in which all the control gains are strictly negative to ensure the closed-loop stability (Nguyen et al., 2017).

The CTC attitude controller (7) implies several robustness problems especially when considering model mismatches, measurement delays and system constraints (Craig, 2005). Therefore, a more advanced control technique must be applied instead. In the next section, we propose an NMPC (Nonlinear Model Predictive Control) controller for tackling the multicopter attitude control problem under state and input constraints. Based on our previous work (Nguyen et al., 2019), the closed-loop stability and also the solution feasibility of the NMPC controller can be derived from the properties of the CTC controller (7).

3. NMPC DESIGN FOR ATTITUDE CONTROL

Controlling a multicopter system requires a hierarchical control design in which, the attitude controller at the low control level tracks the desired angle $\eta_d \triangleq [\phi_d\ \theta_d\ \psi_d]^\top$ sent from the high control level (Nascimento and Saska, 2019). The desired angles η_d are usually and should be considered as step references (i.e., $(\dot{\eta}_d, \ddot{\eta}_d)$ as in (8) are fixed as zero) since differentiating these references potentially introduces large noises to the controlled system under practical considerations (Cao and Lynch, 2016). Hence, in the following, we design an NMPC controller for stabilizing the rotation dynamics (1)–(2) around the equilibrium consisting of the desired angles η_d, the zero angle rate and the zero input torque. This is a particular application of the NMPC design for stabilizing a general "computed-torque like" system with guaranteed stability introduced in Nguyen et al. (2019). We first transform the rotation dynamics (1)–(2) into:

$$\dot{x} = f(x, u), \tag{9}$$

with $x \triangleq [\eta\ \dot{\eta}]^\top \in \mathbb{R}^6$ and $f(\cdot)$ taking the appropriate elements from the "computed-torque like" form (6). The equilibrium point of the dynamics (9) is given by:

$$x_e = [\eta_d\ \mathbf{0}]^\top,\ u_e = \mathbf{0}, \tag{10}$$

with $\eta_d \triangleq [\phi_d\ \theta_d\ \psi_d]^\top$ the angle set-point and $\mathbf{0} \in \mathbb{R}^3$ the zero vector. For the problem to be well-defined, the desired angles need to satisfy the state constraints, i.e., $(|\phi_d|, |\theta_d|) < \phi_{\max}$ as in (4).

The corresponding NMPC optimization problem (OP) at time t is given by:

$$\min_{\bar{u}_t(\cdot)} \int_t^{t+T_p} \Big(\big\|\bar{x}(s) - x_e\big\|^2_Q + \big\|\bar{u}(s)\big\|^2_R\Big) ds + \big\|\bar{x}(t+T_p) - x_e\big\|^2_P \tag{11}$$

subject to:

$$\dot{\bar{x}} = f(\bar{x}, \bar{u}),\ \bar{x}(t) = x(t), \tag{12a}$$

$$\bar{x}(s) \in \mathcal{X},\ \bar{u}(s) \in \mathcal{U},\ s \in [t, t+T_p], \tag{12b}$$

$$\bar{x}(t+T_p) \in \mathcal{X}_f(x_e), \tag{12c}$$

where $T_p \in \mathbb{R}^+$ is the prediction horizon, $\bar{x}(s)$ and $\bar{u}(s)$ are the predicted state and input while $\bar{u}(\cdot)$ stands for the whole predicted input trajectory along $[t, t+T_p]$. The dynamics $f(\cdot)$ are given in (9). The sets $\mathcal{X}$, $\mathcal{U}$ are from (4)–(5) while the terminal region $\mathcal{X}_f(x_e) \in \mathbb{R}^6$ is defined

hereinafter. The weighting matrices $Q,\ P \in \mathbb{R}^{6\times 6}$ and $R \in \mathbb{R}^{3\times 3}$ are all symmetric and positive definite.
Then, the NMPC input at time t is defined as:

$$u_{\text{MPC}}(s,t) = \bar{u}^*(s, x(t), x_e),\ \forall s \in [t, t+\delta], \tag{13}$$

with $\bar{u}^*(s, x(t), x_e)$ with $s \in [t, t+T_p]$ the optimal input resulted from the OP (11)–(12) and δ the sampling time. The closed-loop stability and the recursive feasibility of the NMPC controller (11)–(13) has been established in Mayne et al. (2000); Chen and Allgöwer (1998). They require the design to satisfy four conditions given as follows:

C1: States constraints satisfaction in $\mathcal{X}_f$, i.e.:

$$\mathcal{X}_f \subseteq \mathcal{X},\ x_e \in \mathcal{X}_f. \tag{14}$$

C2: There exists a local controller $u_{\text{loc}}(\boldsymbol{x})$ such that:

$$u_{\text{loc}}(\boldsymbol{x}) \in \mathcal{U},\ \forall x \in \mathcal{X}_f. \tag{15}$$

C3: $\mathcal{X}_f$ is positive invariant under $u_{\text{loc}}(x)$.

C4: $\forall x \in \mathcal{X}_f$, the trajectory of the system (9) under $u_{\text{loc}}(x)$ satisfies:

$$\frac{d}{dt}\left(\|x - x_e\|_P^2\right) + \|x - x_e\|_Q^2 + \|u_{\text{loc}}^2(x)\|_R^2 \leq 0. \tag{16}$$

Furthermore, in Nguyen et al. (2019), the foregoing conditions are particularized using the CTC controller u_{CTC} (7) as the local controller u_{loc}. This allows simpler analysis (resulted from the linearization effect of u_{CTC}) and larger size of the terminal invariant set $\mathcal{X}_f$ employed in (12c) (w.r.t. the result obtained from a standard linear controller as used in Chen and Allgöwer (1998)). The NMPC ingredients proposed in Nguyen et al. (2019) will be introduced particularly for the system (9) in the next section.

4. NMPC PARAMETERS DESIGN USING A LOCAL COMPUTED-TORQUE CONTROLLER

Let us consider a ball $\mathcal{B}$ centered in (x_e, μ_e) and parameterized by a radius $\varepsilon \in \mathbb{R}_+$ as:

$$\mathcal{B}(x_e, \varepsilon) = \left\{(x,\mu)|\ \|x - x_e\|^2 + \|\mu - \mu_e\|^2 \leq \varepsilon^2\right\}, \tag{17}$$

with x_e as in (10), μ the virtual input as in (8) and $\mu_e = \mathbf{0}$ (as $\ddot{\eta}_d = \mathbf{0}$ for set-point tracking). The main ideas given in Nguyen et al. (2019) are first to establish the condition on ε such that the set $\mathcal{B}(x_e, \varepsilon)$ from (17) is input constraint admissible and then, to choose the control gains as in (8) to make the set $\mathcal{B}(x_e, \varepsilon)$ also invariant. However, various elements of the setup are constructed depending on the angle set-point η_d (via x_e as in (10)) which is received from the high control level and hence, is not known beforehand. This significantly increases the complexity of the on-line procedure since it has to complete the design first and then, to solve the NMPC optimization problem (11). Note that, similar problems also occur for other NMPC design approaches in the literature (Chen and Allgöwer, 1998; Mayne et al., 2000) as the terminal constraint sets are all constructed around the equilibrium. Therefore, this section will recapitulate parts of the results published in Nguyen et al. (2019) and also present the original contributions on how we reduce the dependence of the controller setup on the equilibrium x_e (10) in order to overcome the aforementioned difficulties.

4.1 Input constraint admissible set

Proposition 2. Let us define two vectors C and M, both in $\mathbb{R}^3$, as follows:

$$C = \begin{bmatrix} J_x\sqrt{1+\mathrm{s}^2\,\phi_{\max}} & J_y & J_z \end{bmatrix}^\top, \tag{18}$$

$$M = \frac{1}{2}\begin{bmatrix} J_x + 2|J_z - J_y| \\ 2J_y + 2\sqrt{1+\mathrm{s}^2\,\phi_{\max}}|J_z - J_x| \\ 2J_z + 2\sqrt{1+\mathrm{s}^2\,\phi_{\max}}|J_x - J_y| \end{bmatrix}, \tag{19}$$

with $J = \text{diag}(J_x, J_y, J_z)$ the inertial matrix as in (2) and $\phi_{\max}$ the maximum angle as in (4). Next, we further define $\varepsilon_{\max}$ as the largest possible positive scalar such that:

$$C\varepsilon_{\max} + M\varepsilon_{\max}^2 \leq u_{\max}, \tag{20}$$

with $u_{\max}$ as in (5). Then, for all $(x,\mu) \in \mathcal{B}(x_e, \varepsilon)$ as in (17) and with $\varepsilon \leq \varepsilon_{\max}$, the followings hold:

$$\|u_{\text{CTC}} - u_e\|^2 \leq \mathsf{L}(\|x - x_e\|^2 + \|\mu - \mu_e\|^2), \tag{21}$$

$$u_{\text{CTC}} \in \mathcal{U}, \tag{22}$$

with u_{CTC} the CTC controller from (7), (x_e, u_e) as in (10), $\mu_e = \mathbf{0}$, $\mathcal{U}$ the input constraint set from (5) and the scalar L defined as follows:

$$\mathsf{L} = \|C + M\varepsilon\|^2, \tag{23}$$

with $C,\ M$ as in (18)–(19).

Proof. The proof starts by applying Taylor's approximation to the CTC controller u_{CTC} from (7) around (x_e, μ_e) as similar to the work in Nguyen et al. (2019):

$$u_{\text{CTC}} = u_e + {}^x\boldsymbol{J}(x - x_e) + {}^\mu\boldsymbol{J}(\mu - \mu_e) + \mathcal{R}(x, \mu, x_e), \tag{24}$$

with the two Jacobians ${}^x\boldsymbol{J} = (\partial u_{\text{CTC}})/(\partial x)(x_e, \mu_e) = 0_{6\times 6}$ and ${}^\mu\boldsymbol{J} = (\partial u_{\text{CTC}})/(\partial \mu)(x_e, \mu_e) = JW(\eta_d)$ (i.e. $W(\eta_d)$ the matrix W as in (3) given in terms of the desired angle η_d). By applying Cauchy-Schwarz inequality, we obtain:

$$|{}^x\boldsymbol{J}(x - x_e) + {}^\mu\boldsymbol{J}\mu| \leq C(x_e)\sqrt{\|x - x_e\|^2 + \|\mu\|^2}, \tag{25}$$

in which, $C(x_e)$ is given by:

$$\mathcal{C}(x_e) = \begin{bmatrix} J_x\sqrt{1+\mathrm{s}^2\,\theta_d} \\ J_y\sqrt{\mathrm{c}^2\,\phi_d + \mathrm{s}^2\,\phi_d\,\mathrm{c}^2\,\theta_d} \\ J_z\sqrt{\mathrm{s}^2\,\phi_d + \mathrm{c}^2\,\phi_d\,\mathrm{c}^2\,\theta_d} \end{bmatrix} \leq C, \tag{26}$$

with C as in (18). The latter inequality holds for all $(\phi_d, \theta_d) \leq \phi_{\max}$ from (4).
Next, the explicit formulation of the remainder term $\mathcal{R}(x, \mu, x_e)$ from (24) is as follows:

$$\mathcal{R}(x, \mu, x_e) = u_{\text{CTC}} - JW(\eta_d)\mu, \tag{27}$$

As detailed in Appendix A, for all $(\phi_d, \theta_d) \leq \phi_{\max}$ from (4), we have that:

$$|\mathcal{R}(x, \mu, x_e)| \leq M\left(\|x - x_e\|^2 + \|\mu - \mu_e\|^2\right), \tag{28}$$

with the vector $M \in \mathbb{R}^3$ defined in (19). Then, introducing (25), (28) to (24) and using $\|x - x_e\|^2 + \|\mu\|^2 \leq \varepsilon^2, \forall (x,\mu) \in \mathcal{B}(x_e, \varepsilon)$ lead to:

$$|u_{\text{CTC}} - u_e| \leq (C + M\varepsilon)\sqrt{\|x - x_e\|^2 + \|\mu\|^2},$$

which further proves the two assertions (21)–(22) and hence, completes the proof. □

Remark 3. In Nguyen et al. (2019), for finding the maximum radius $\varepsilon_{\max}$ as in (32), the varying term $\mathcal{C}(x_e)$ as in (26) is employed instead of the constant term C from (18). Furthermore, the remainder term $\mathcal{R}(x, \mu, x_e)$ as in (27) is bounded by exploiting the Hessian matrix containing all the second-order partial derivatives of the CTC controller u_{CTC} from (7). The approach requires to construct all the elements as well as to calculate again the maximum radius $\varepsilon_{\max}$ as in (32) at each time step, hence, being inappropriate for the attitude control problem which requires fast solutions. □

4.2 Constraint admissible invariant set

Let us construct the control gain matrix K as:

$$K = \left[\text{diag}(K_\phi, K_\theta, K_\psi) \;\; \text{diag}(K_{\dot\phi}, K_{\dot\theta}, K_{\dot\psi})\right], \quad (29)$$

with the control gains as in (8). Then, the virtual PD input μ as in (8) is shortened into $\mu = K(x - x_e)$. Using this, the set $\mathcal{B}(x_e, \varepsilon)$ from (17) becomes:

$$\mathcal{B}(x_e, \varepsilon) = \left\{(x - x_e)^\top (\boldsymbol{I}_6 + K^\top K)(x - x_e) \le \varepsilon^2\right\}, \quad (30)$$

with $\boldsymbol{I}_6$ the 6×6 identity matrix.

Proposition 4. (Nguyen et al. (2019)).
Let us choose the control gains $K_p,\ K_{\dot p}$ with $p \in \{\phi, \theta, \psi\}$ as in (29) such that:

$$\begin{cases} K_p < 0,\ K_{\dot p} < 0, \\ 4K_{\dot p}^2 > -K_p(K_p + 1)^2 - K_p - \dfrac{(K_p + 1)^2}{K_p}, \end{cases} \quad (31)$$

and also choose the radius ε as in (30) such that:

$$\begin{cases} \varepsilon \le \varepsilon_{\max}, \\ \mathcal{B}(x_e, \varepsilon) \subseteq \mathcal{X}, \end{cases} \quad (32)$$

with $\varepsilon_{\max}$ satisfying (32). Then, the set $\mathcal{B}(x_e\varepsilon)$ from (30) is constraint admissible and positive invariant for the rotation dynamics (9) under the CTC controller (7). □

Proof. The proof is detailed in Nguyen et al. (2019). □

The condition $\mathcal{B}(x_e, \varepsilon) \subseteq \mathcal{X}$ from (32) brings difficulties due to the nonlinear relation $\omega = W\dot\eta$ from (1). Therefore, in the following, we propose an alternative approach for efficiently choosing ε such that (32) is satisfied.

Corollary 5. (Efficient choice of ε). The conditions (32) holds for all $\varepsilon \in \mathbb{R}_+$ satisfying:

$$\varepsilon \le \min\left\{\varepsilon_{\max}, \phi_{\max} - \max\{|\phi_d|, |\theta_d|\}, \frac{\omega_{\max}}{\sqrt{1 + \sin^2\phi_{\max}}}\right\}, \quad (33)$$

with $\varepsilon_{\max}$ as in (20), $\phi_{\max},\ \omega_{\max}$ as in (4) and $\phi_d,\ \theta_d$ the desired roll, pitch angles sent from high control level.

Proof. At first, $\varepsilon \le \varepsilon_{\max}$ is as required in (32).
Next, introducing $\varepsilon \le \phi_{\max} - \max\{\phi_d, \theta_d\}$ to the formulation of $\mathcal{B}(x_e, \varepsilon)$ as in (17) leads to:

$$\|\eta - \eta_d\| \le \phi_{\max} - \max\{|\phi_d|, |\theta_d|\}, \quad (34)$$

which further provides:

$$(|\phi - \phi_d|, |\theta - \theta_d|) \le \phi_{\max} - \max\{|\phi_d|, |\theta_d|\}. \quad (35)$$

Then, the angle constraints as required in (4) are satisfied. Similarly, choosing $\varepsilon \le \omega_{\max}/\sqrt{1 + \text{s}^2\,\phi_{\max}}$ is to ensure:

$$\|\dot\eta\| \le \frac{\omega_{\max}}{\sqrt{1 + \text{s}^2\,\phi_{\max}}}, \quad (36)$$

which further guarantees the constraints $(|\omega_x|, |\omega_y|) \le \omega_{\max}$ as detailed in Appendix A. □

4.3 Terminal weighting matrix and closed-loop stability

This section completes the NMPC design (11)–(13) by providing the choice of the terminal weighting matrix P as employed in (11) and the proof for the closed-loop stability of the controller.

Proposition 6. (NMPC design with guaranteed stability). The NMPC design (11)-(22) for stabilizing the system (9) achieves the recursive feasibility and closed-loop stability with the ingredients defined as follows:

- The terminal region $\mathcal{X}_f$ employed in (12c) is taken as the set $\mathcal{B}(q_e, \boldsymbol{\varepsilon})$ from (30) satisfying Proposition 4
- The terminal weighting matrix $P \in \mathbb{R}^{6\times6}$ from (11) is obtained as the unique solution of the following Lyapunov equation:

$$A_K^\top P + P A_K + Q + R^* = \boldsymbol{0}, \quad (37)$$

in which, $A_K = [0_{3\times3}\ \boldsymbol{I}_3; K] \in \mathbb{R}^{6\times6}$ (K as in (29)) is the stable matrix resulted from introducing the CTC controller (24) to the system (9), Q is from (11) and $R^* \in \mathbb{R}^{6\times6}$ the symmetric matrix satisfies:

$$R^* \succeq \max(\text{eig}(R))\mathsf{L}(\boldsymbol{I}_6 + K^\top K), \quad (38)$$

with L from (23) and the matrix K from (29).

Proof. The design proposed in Proposition 6 satisfies four requirements **C1**–**C4** (c.f. Section 3) on designing an NMPC. The first three conditions **C1**–**C3** are clearly satisfied by using $\mathcal{B}(x_e, \varepsilon)$ from (30) (constraint admissible and positive invariant), as the terminal constraint set. Then, regarding the fourth condition **C4**, we have that:

$$\frac{d}{dt}\left(\|x - x_e\|_P^2\right) = (x - x_e)^\top (A_K^\top P + A_K P)(x - x_e), \quad (39)$$

with $A_K = [0_{3\times3}\ \boldsymbol{I}_3; K] \in \mathbb{R}^{6\times6}$ and K from (29)). Next, the input term is bounded by:

$$\|u_{\text{CTC}}\|_R^2 \le \max(\text{eig}(R))\|u_{\text{CTC}}\|^2 \le \|x - x_e\|_{R^*}^2, \quad (40)$$

in which, the latter inequality is due to $\|u_{\text{CTC}}\|^2 \le \mathsf{L}(x - x_e)^\top(\boldsymbol{I}_6 + K^\top K)(x - x_e)$ from (21). Then, introducing (39)–(40) to condition **C4** (16) leads to:

$$\begin{aligned} &\text{LHS of (16)} \\ &\le (x - x_e)^\top \underbrace{(A_K^\top P + A_K P + Q + R^*)}_{=0 \text{ due to (37)}}(x - x_e). \end{aligned} \quad (41)$$

This also completes the proof. □

4.4 Summary of the NMPC design using CTC as a local controller

This section summarizes the design procedure and the functioning scheme of the NMPC controller in (11)–(13) for angle set-point tracking of the model (1)–(2).

Procedure 1. (**Off-line preparation stage**).

1) Choose the symmetric positive definite matrices $Q \in \mathbb{R}^{6\times6}$ and $R \in \mathbb{R}^{3\times3}$ as in (11).

2) Choose the prediction horizon T_p based on the computational constraint of the platform.

3) Find the largest possible $\varepsilon_{\max}$ satisfying (20) and L as in (23).

4) Define the matrices K as in (29) satisfying (31).

5) Define the symmetric matrix R^* satisfying (38), then, solve the Lyapunov equation (37) for the terminal weighting matrix P. □

Procedure 2. (**On-line solving stage**).

1) Receive the angle set-point η_d from the high control level (10).

2) Choose ε as in (33) to obtain the terminal region $\mathcal{B}(x_e, \varepsilon)$ from (30).

3) Measure the state, solve the NMPC OP (11)–(12) and provide the input, u_{MPC} as in (13) to the system (1)–(2).□

5. SIMULATION RESULTS

We consider the simulation model of the rotation dynamics (1)–(5) characterized by the following numerical values:

- $J = \text{diag}\{1.4\ 1.4\ 2.2\} \times 10^{-5}$ [kgm^2] as used in (2).
- $\phi_{\max} = 5^\circ$, $\omega_{\max} = 2$ rad/s as used in (4).
- $u_{\max} = [43\ 43\ 17]^\top \times 10^{-4}$ N/m as used in (5).

The requirement is to track the desired angle set-points $\eta_d = [\phi_d\ \theta_d\ \psi_d]^\top$ given in Fig. 1 which are obtained by applying the zero-order hold method with the holding time of 0.1 seconds for discretizing a smooth reference. The NMPC controller is simulated at the sampling time of $\delta = 0.01$ seconds while the prediction horizon is chosen as $T_p = 0.05$ seconds, thus, having 5 steps. The optimization problem in (11) is solved with solver IPOPT (Wächter and Biegler, 2006) in Python. All the parameters related to the off-line preparation stage given in Procedure 1 are gathered in Table 1.

Table 1. Parameters prepared off-line of the NMPC controller (11) following Procedure 1.

Parameters	Value
C as in (18)	$[14.05\ 14\ 22]^\top 10^{-6}$
M as in (19)	$[30\ 44.6\ 44]^\top 10^{-6}$
$\varepsilon_{\max}$ as in (20)	8.3047
L as in (23)	10^{-7}
K as in (29), (31)	$[-0.5\boldsymbol{I}_3\ \ -0.8\boldsymbol{I}_3]$
Q as in (11)	$\text{diag}\{1, 1, 1, 0.1, 0.1, 0.1\}$
R as in (11)	$0.01\boldsymbol{I}_3$
R^* as in (38)	$\begin{bmatrix} 12.53\boldsymbol{I}_3 & 4\boldsymbol{I}_3 \\ 4\boldsymbol{I}_3 & 16.44\boldsymbol{I}_3 \end{bmatrix} 10^{-10}$
P as in (37)	$\begin{bmatrix} 1.46\boldsymbol{I}_3 & \boldsymbol{I}_3 \\ \boldsymbol{I}_3 & 1.31\boldsymbol{I}_3 \end{bmatrix}$

At each on-line simulation step, after taking the angle references η_d (thin step lines in Fig. 1), the controller first chooses the radius ε as in (33) which is plotted in Fig. 2. Then, the NMPC controller solves the OP (11) and provides the inputs $u \triangleq [u_\phi\ u_\theta\ u_\psi]^\top$ as shown in Fig. 4. The angle tracking results are shown in Fig. 1 in which the simulation angles plotted by thick lines (red for ϕ, green for θ and blue for ψ) closely track their piece-wise constant references given in thin lines with according colors. The angular velocities are given in Fig. 3 in which we observe a slight chattering phenomenon (can also be seen from the torques plotted in Fig. 4). This chattering problem is caused by the controller's effort to stabilize the angular velocities and the torques at their zero equilibrium values as in (10). Through multiple simulations, we find that this issue is aggravated by increasing the value of the matrix R as in (11). Thus, we have reduced this phenomenon by decreasing the value of R and also the gain of the angular velocities within the cost function (11) as shown in Table 1 (i.e., 0.1 for ω and 0.01 for u in comparison with 1 for the angle η). The issue can be further mitigated by adding a penalty on the input variation to the cost as proposed in Badgwell and Qin (2015). It also should be clarified that all the states and inputs validates their constraints given in (4)–(5) due to the usage of the NMPC algorithm.

Fig. 1. Angle tracking results.

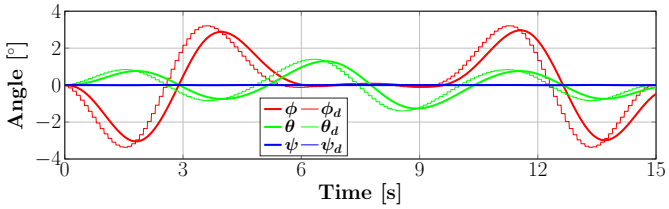

Fig. 2. Radius ε as in (33).

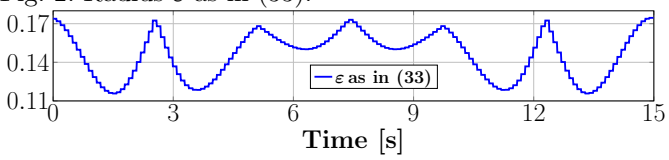

Fig. 3. Angular velocities.

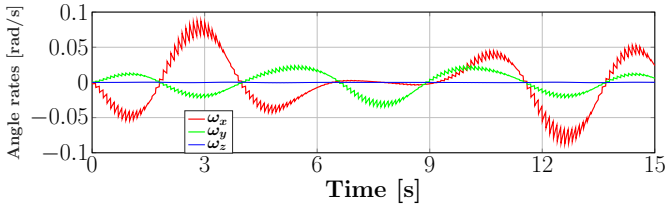

Fig. 4. Torque values.

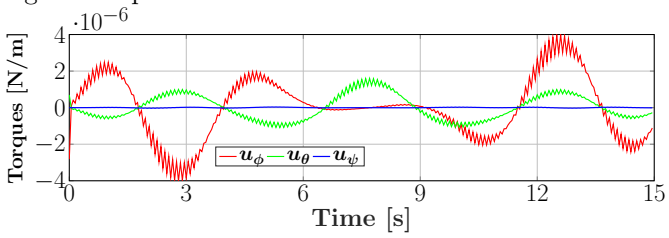

Beside the tracking results, the computing time per step is also important for the NMPC controller. Table 2 gathers the computing time per step for the whole simulation, i.e., 1500 steps. The average computing time is 54 ms while the minimum value reaches 30.9 ms. Note that, the maximum value of 93.7 ms only happens once at the first step when the solver is setting up the algorithm. We

Table 2. Information on the computing time of the NMPC controller designed for set-point angle tracking.

	Mean	Min	Max	Standard deviation
Value [ms]	54	30.9	93.7	10

notice that the computing time is larger than the chosen sampling time $\delta = 0.1$ seconds, hence, this setup (including both the formulation of the OP (11) and the employed hardware) is not ready for a real implementation. However, we are confident that applying some existing speeding-up approaches can mitigate the issue. E.g., in Zanelli et al. (2018), the authors succeed in embedding the OP (11) into a low-power micro controller by re-formulating the problem into its approximated quadratic formulation and then, solving it by using a modified interior-point method.

6. CONCLUSION

This paper presented the design of an NMPC controller for attitude set-point angle tracking of the multicopter

system. It employed a CTC (computed-torque control) local controller to guarantee the NMPC scheme's closed-loop stability and feasibility. We provided several alternative designs for the NMPC ingredients (in comparison with the original contributions given in our previous work (Nguyen et al., 2019)) such as the Lipschitz constant and the radius of the terminal region. We reduce the dependence of the design on the desired set-points received from the high control level since they are not known in advance, and hence, we are able to reduce the complexity for on-line computation. Simulations over a quadcopter model validate the theoretical results. Future works will concentrate on implementing the proposed controller into a microprocessor and conducting experimental tests.

REFERENCES

Badgwell, T.A. and Qin, S.J. (2015). Model-predictive control in practice. *Encyclopedia of Systems and Control*, 756–760.

Cao, N. and Lynch, A.F. (2016). Inner–outer loop control for quadrotor uavs with input and state constraints. *IEEE Transactions on Control Systems Technology*, 24(5), 1797–1804.

Chen, H. and Allgöwer, F. (1998). A quasi-infinite horizon nonlinear model predictive control scheme with guaranteed stability. *Automatica*, 34(10), 1205–1217.

Craig, J.J. (2005). *Introduction to robotics: mechanics and control*, volume 3. Pearson/Prentice Hall Upper Saddle River, NJ, USA:.

Freddi, A., Lanzon, A., and Longhi, S. (2011). A feedback linearization approach to fault tolerance in quadrotor vehicles. *IFAC Proceedings Volumes*, 44(1), 5413–5418.

Gros, S., Quirynen, R., and Diehl, M. (2012). Aircraft control based on fast non-linear mpc & multiple-shooting. In *51st IEEE Conference on Decision and Control (CDC)*, 1142–1147. IEEE.

Hehn, M. and D'Andrea, R. (2015). Real-time trajectory generation for quadrocopters. *IEEE Transactions on Robotics*, 31(4), 877–892.

Lewis, F.L., Dawson, D.M., and Abdallah, C.T. (2003). *Robot manipulator control: theory and practice*. CRC Press.

Mayne, D.Q., Rawlings, J.B., Rao, C.V., and Scokaert, P.O. (2000). Constrained model predictive control: Stability and optimality. *Automatica*, 36(6), 789–814.

Mogili, U.R. and Deepak, B. (2018). Review on application of drone systems in precision agriculture. *Procedia computer science*, 133, 502–509.

Nascimento, T.P. and Saska, M. (2019). Position and attitude control of multi-rotor aerial vehicles: A survey. *Annual Reviews in Control*.

Nguyen, N.T., Prodan, I., and Lefèvre, L. (2019). On the use of a computed-torque control law for the terminal region of an nmpc scheme. In *Proc. 2019 American Control Conference (ACC'19)*, 1008–1013.

Nguyen, N.T., Prodan, I., Stoican, F., and Lefèvre, L. (2017). Reliable nonlinear control for quadcopter trajectory tracking through differential flatness. *IFAC-PapersOnLine*, 50(1), 6971–6976.

Wächter, A. and Biegler, L.T. (2006). On the implementation of an interior-point filter line-search algorithm for large-scale nonlinear programming. *Mathematical programming*, 106(1), 25–57.

Zanelli, A., Horn, G., Frison, G., and Diehl, M. (2018). Nonlinear model predictive control of a human-sized quadrotor. In *2018 European Control Conference (ECC)*, 1542–1547. IEEE.

Appendix A. BOUND OF THE TAYLOR'S REMAINDER $\mathcal{R}(\cdot)$ FROM (27)

The remainder $\mathcal{R}(x, \mu, x_e)$ as in (27) is explicitly given by:

$$\mathcal{R}(x, \mu, x_e) = J(W - W(\eta_d))\mu + J\dot{W}\dot{\eta} + \omega \times (J\omega), \quad \text{(A.1)}$$

in which, $\omega = W\dot{\eta}$ as in (1) leads to:

$$\omega_x = \dot{\phi} - \dot{\psi}\,\mathrm{s}\,\theta, \quad \text{(A.2)}$$

$$\omega_y = \dot{\theta}\,\mathrm{c}\,\phi + \dot{\psi}\,\mathrm{s}\,\phi\,\mathrm{c}\,\theta, \quad \text{(A.3)}$$

$$\omega_z = -\dot{\theta}\,\mathrm{s}\,\phi + \dot{\psi}\,\mathrm{c}\,\phi\,\mathrm{c}\,\theta. \quad \text{(A.4)}$$

Next, applying Cauchy-Schwarz inequality to (A.2)–(A.3) leads to:

$$|\omega_x| \leq \sqrt{(1 + \mathrm{s}^2\,\theta)(\dot{\phi}^2 + \dot{\psi}^2)} \leq \sqrt{1 + \mathrm{s}^2\,\phi_{\max}}\|\dot{\eta}\|, \quad \text{(A.5)}$$

$$|\omega_y| \leq \sqrt{(\mathrm{c}^2\,\phi + \mathrm{s}^2\,\phi\,\mathrm{c}^2\,\theta)(\dot{\theta}^2 + \dot{\psi}^2)} \leq \|\dot{\eta}\|, \quad \text{(A.6)}$$

$$|\omega_z| \leq \sqrt{(\mathrm{s}^2\,\phi + \mathrm{c}^2\,\phi\,\mathrm{c}^2\,\theta)(\dot{\theta}^2 + \dot{\psi}^2)} \leq \|\dot{\eta}\|, \quad \text{(A.7)}$$

in which, the second inequality of (A.5) is due to $|\theta| \leq \phi_{\max}$ as constrained in (4) and to the fact that sin is monotonously increasing on the interval $[0, \pi/2]$. Also, (A.6) and (A.7) come by using $\mathrm{c}^2\,\phi + \mathrm{s}^2\,\phi = 1$.

Next, let us denote $\mathcal{R} \triangleq [\mathcal{R}_1\ \mathcal{R}_2\ \mathcal{R}_3]^\top$ and $\mu = [\mu_1\ \mu_2\ \mu_3]^\top$. From (A.1), we have that:

$$\mathcal{R}_1 = -J_x\left((\mathrm{s}\,\theta - \mathrm{s}\,\theta_d)\mu_3 + \dot{\theta}\dot{\psi}\,\mathrm{c}\,\theta\right) + (J_z - J_y)\omega_y\omega_z, \quad \text{(A.8)}$$

in which, the elements are bounded as follows:

- $$|(\mathrm{s}\,\theta - \mathrm{s}\,\theta_d)\mu_3| = \left|2\,\mathrm{s}\left(\frac{\theta - \theta_d}{2}\right)\mathrm{c}\left(\frac{\theta + \theta_d}{2}\right)\mu_3\right| \leq \left|2\,\mathrm{s}\left(\frac{\theta - \theta_d}{2}\right)\mu_3\right| \leq \frac{1}{2}\left(4\,\mathrm{s}^2\left(\frac{\theta - \theta_d}{2}\right) + \mu_3^2\right) \leq \frac{1}{2}\left((\theta - \theta_d)^2 + \mu_3^2\right). \quad \text{(A.9)}$$
- $$\left|\dot{\theta}\dot{\psi}\,\mathrm{c}\,\theta\right| \leq \left|\dot{\theta}\dot{\psi}\right| \leq \frac{1}{2}\left(\dot{\theta}^2 + \dot{\psi}^2\right). \quad \text{(A.10)}$$

Then, introducing (A.9)–(A.10) and (A.6)–(A.7) to (A.8) leads to:

$$|\mathcal{R}_1| \leq \frac{J_x}{2}\left((\theta - \theta_d)^2 + \mu_3^2 + \dot{\theta}^2 + \dot{\psi}^2\right) + |J_y - J_z|\|\dot{\eta}\|^2, \leq \left(\frac{J_x}{2} + |J_y - J_z|\right)\left(\|\eta - \eta_d\|^2 + \|\dot{\eta}\|^2 + \|\mu\|^2\right). \quad \text{(A.11)}$$

Due to the limit on space, we will provide only the proof for $\mathcal{R}_1$ since those of the others can be obtained similarly. Furthermore, using (A.5)–(A.6), we can also prove that the constraints on angle rates: $(|\omega_x|, |\omega_y|) \leq \omega_{\max}$ as in (4) are satisfied if:

$$\|\dot{\eta}\| \leq \omega_{\max}/\sqrt{1 + \mathrm{s}^2\,\phi_{\max}}, \quad \text{(A.12)}$$

with $\phi_{\max}$ the maximum angle value from (4). The proof is obtained by simply introducing (A.12) to (A.5)–(A.6) which ultimately leads to $(\omega_x|, |\omega_y|) \leq \omega_{\max}$.